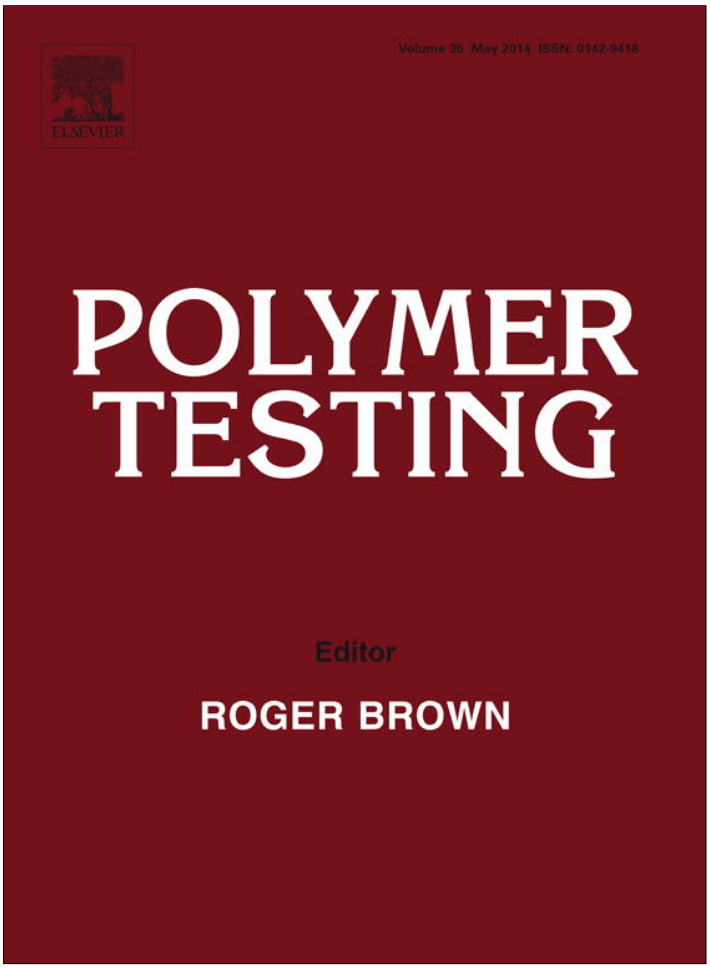

Polymer Testing 35 (2014) 92–100

Contents lists available at ScienceDirect

Polymer Testing

journal homepage: www.elsevier.com/locate/polytest

Material properties

Thermal, viscoelastic and mechanical behavior of polypropylene with synthetic boehmite alumina nanoparticles

D. Pedrazzoli [a,*], V.M. Khumalo [b,c], J. Karger-Kocsis [c,d,e], A. Pegoretti [a]

[a] Department of Industrial Engineering and INSTM Research Unit, University of Trento, Trento 38123, Italy
[b] Polymers and Composites, Materials Science and Manufacturing, Council for Scientific and Industrial Research, CSIR, P.O. Box 395, Pretoria 0001, South Africa
[c] Polymer Technology, Faculty of Mechanical Engineering and Built Environment, Tshwane University of Technology, Pretoria 0001, South Africa
[d] MTA–BME Research Group for Composite Science and Technology, Muegyetem rkp. 3., H-1111 Budapest, Hungary
[e] Polymer Engineering, Faculty of Mechanical Engineering, Budapest University of Technology and Economics, H-1111 Budapest, Hungary

ARTICLE INFO

Article history:
Received 27 January 2014
Accepted 6 March 2014

Keywords:
Nanocomposite
Boehmite alumina
Morphology
Thermal properties
Mechanical properties
Tear resistance

ABSTRACT

Effects of nanofiller concentration and surface treatment on the morphology, thermal, viscoelastic and mechanical behavior of polypropylene copolymer (PP)/boehmite alumina (BA) nanocomposites were investigated. Both untreated BA particles and those treated with octylsilane (OS) or sulphonic acid compound (OS2) were added at up to 10 wt% to produce nanocomposites by melt mixing followed by film blow molding and hot pressing. Dispersion of BA was studied by scanning electron microscopy. Differential scanning calorimetry and wide-angle X-ray scattering were adopted to detect changes in the crystalline structure of PP. Thermooxidative degradation of the nanocomposites was assessed by thermogravimetrical analysis. Dynamic mechanical analysis served for studying the viscoelastic properties, whereas quasi-static tensile, creep and Elmendorf tear tests were used to detect changes in the mechanical performance. BA nanoparticles were finely dispersed in PP up to 10 wt%, even when they were not surface modified. The resistance to thermal degradation was markedly improved by BA nanomodification. Since the crystalline characteristics of the PP matrix did not practically change with BA modification, changes observed in the mechanical properties were attributed to BA dispersion, filler/matrix interactions and related effects.

1. Introduction

Increasing efforts are devoted to the research of thermoplastic nanocomposites exhibiting improved and novel properties. Most of these studies are focused on the investigation of correlations between structural features and mechanical properties [1–3]. In particular, considerable resources have been dedicated to research of thermoplastic matrices modified with polar nanofillers (such as silicas, metal oxides, metal salts, layered silicates, etc.) in order to enhance their thermal, mechanical and rheological performance [4–8]. On the other hand, these nanofillers are generally poorly dispersed in apolar thermoplastics (such as polyolefins), thus limiting their beneficial effects on the target thermo-mechanical properties. In order to enhance the dispersibility of nanofillers in polyolefins they are usually introduced after appropriate surface treatment [9–11] or together with suitable polymeric compatibilizers

* Corresponding author. Tel.: +39 0461 282411; fax: +39 0461 281977.
E-mail addresses: d.pedrazzoli@ing.unitn.it, pedrazzoli.diego@gmail.com (D. Pedrazzoli).

http://dx.doi.org/10.1016/j.polymertesting.2014.03.003
0142-9418/

[12–16]. Nevertheless, with the aim of avoiding additional costs and processes, researchers have been looking for nanofillers which can be easily and homogeneously dispersed in the polymeric matrix without use of compatibilizers or surface treatments.

In this respect, synthetic boehmite alumina (BA), with chemical composition n-AlO(OH), represents an ideal candidate thanks to its inexpensive and easy production process [17–20]. Its primary particle size is in the range of tens of nanometers.

BA has recently become the subject of research attention as a new type of additive for enhancing the mechanical, thermal and fire-retardant performances of polymers [21–25]. In order to get a deeper understanding on the structure-property relationships, two BA grades with different primary particle size were incorporated in both low-density and high-density polyethylene (LDPE and HDPE, respectively) by melt compounding. It was found that BA was dispersed at the nanoscale within these matrices and did not influence the rheological properties of the corresponding PEs. On the other hand, BA dramatically enhanced the resistance to thermo-oxidative degradation of PEs [19]. Furthermore, it was found that BA worked as reinforcing filler according to quasi-static mechanical tests and dynamic mechanical thermal analysis (DMTA). Interestingly, the perforation impact resistance of PEs nanocomposites was reduced with increasing BA content, with higher primary particle size of the used BA producing less reduction [20].

Polypropylene (PP) does not include any polar group in its backbone that could interact with BA [26], resulting in limited dispersion of the BA in the PP matrix and in poor interfacial adhesion between filler and matrix. This is usually accompanied by limited reinforcing effects. Nevertheless, the compatibilization strategies between BA and thermoplastic matrices include the addition of polymeric compatibilizers [12–15] and the pre-treatment of fillers with coupling agents [27–31]. In particular, Özdilek et al. investigated the effects of both untreated and surface treated BA on the thermo-mechanical behavior and morphology of polyamide 6 (PA 6) nanocomposites, showing that the polymer crystalline structure is significantly changed and the storage modulus is doubled with inclusion of BA particles [18,23]. Ogunniran studied the effect of the incorporation of BA in PP/PA 12 blends, finding that the degree of compatibility of the two polymers increased at high nanoparticle loading, and that BA significantly improved the thermal and mechanical properties [18,32]. In a previous work of our group the influence of BA content and surface treatment was investigated with respect to the morphology, crystallization behavior and mechanical properties of PP copolymer nanocomposites [33]. Specifically, the effects of untreated and surface modified (with octylsilane and sulphonic acid compound, respectively) BA nanoparticles with a crystallite size of around 80 nm on the thermo-mechanical properties were investigated.

The present work is aimed at studying how the addition of BA nanoparticles with crystallite size of 40 nm with and without surface functionalization affects the morphology, thermal and mechanical properties of PP copolymer nanocomposites. BA was incorporated up to 10 wt% in untreated, octylsilane (OS) and alkylbenzene sulphonic acid (OS2) modified forms. In addition to static tensile, the mechanical tests also covered creep and tear resistance of the related nanocomposites, which are rarely addressed.

2. Experimental section

2.1. Materials and samples preparation

A polypropylene impact copolymer, namely CHR 440 type of Sasol (Sasolburg, South Africa), was selected as polymer matrix. Its melt flow index measured at 230 °C and 2.16 kg was 1.5 g/10 min and its density 0.905 $g \cdot cm^{-3}$. Synthetic boehmite Disperal®40, provided by Sasol GmbH (Hamburg, Germany), was used as nanofiller in pristine (BA40) and in surface treated forms. Surface functionalization was performed by octylsilane (BA40-OS) or by C10–C13 alkylbenzene sulphonic acid (BA40-OS2). The nominal primary crystallite size of the pristine form is 40 nm, while the specific surface area is 105 $m^2\ g^{-1}$ [19]. BA was incorporated into the PP matrix at 2.5, 5 and 10 wt %. The unfilled matrix was denoted as PP, while the code of the nanocomposites indicated the matrix, the filler weight amount and filler type. For instance, a sample filled with 5 wt% octylsilane-treated BA is indicated as PP/5BA40-OS.

Samples were prepared by melt mixing using a Berstorff co-rotating twin-screw extruder (ZE-40, Berstorff, Hannover, Germany) followed by granulation. The barrel temperatures from the hoper to die were 185, 185, 195, 195, 205, 205, 220, 220 °C, the screw rotated at 100 rpm and the melt passed through the extruder in about 80 s. The granules were subsequently blow-molded (extruder-film blowing machine, 25 mm extruder type, model LE25-30/CV of Labtech Engineering, Bangkok, Thailand) in order to produce film sheets with thickness of around 0.6 mm. The barrel temperatures from the hopper to die were 180, 185, 190, 195, 200 °C, the screw rotated at 65 rpm and the pressure was 21 MPa. The die temperatures were 200, 210, 220 °C. The rolling speeds of nip and pulling rollers were 3.1 and 3.8 m min^{-1}, respectively, while the blower pressure was set to 0.4 MPa. The specimens used for DMTA were cut from the blow-molded sheets along the machine direction, while the specimens necessary for the Elmendorf tear test were obtained along both machine and transverse directions.

Bulk specimens, necessary for the quasi-static tensile tests, were produced by compression molding of the granules using a P.H.I. hydraulic press (Pasadena Hydraulics Inc, La Puente, CA, USA) in order to produce square sheets with thickness of 4.2 mm. The material was heated to 190 °C while applying a pressure of 25 MPa for 15 min and then cooled to room temperature by water flow.

2.2. Experimental

2.2.1. Spectroscopy analysis

Dispersion of the BA nanoparticles was inspected on the cryo-fractured surfaces of the nanocomposites by scanning

electron microscope (SEM; JEOL JSM-6380LA, Tokyo - Japan). Their electric conductivity was guaranteed by sputtering with an Au/Pd alloy.

2.2.2. Diffraction analysis

Wide angle X-ray scattering (WAXS) spectra were taken by a Phillips® (PANalytical, Almelo, The Netherlands) diffractometer, using CuK_α irradiation (0.154056 nm). Typical scans were performed within a 2θ range between 5° and 40° and sampling interval of 0.02°.

2.2.3. Thermal analyses

Differential scanning calorimetry (DSC) was carried out by a Q2000 (TA Instruments®, New Castle, USA) differential scanning calorimeter under a constant nitrogen flow of 25 ml min^{-1}. Samples were heated to 200 °C at a rate of 10 °C min^{-1} and cooled to 0 °C at a rate of 10 °C min^{-1}. A second heating scan was then performed at 10 °C min^{-1}. Each endothermal peak was characterized by two temperatures, namely peak maximum ($T_{m,max}$) and final melting ($T_{m,final}$), and the crystallinity value ($\varkappa_m$). The latter was estimated by taking the weight fraction of PP in the composites into account and assuming that the melting enthalpy of the 100% crystalline isotactic PP is equal to $\Delta H^0 = 209$ J g^{-1} [34]. Also, the crystallization behavior was characterized by two temperatures, namely peak maximum ($T_{c,max}$) and the initial temperature of crystallization ($T_{c,initial}$). The crystallinity value ($\varkappa_c$), on cooling, was determined as the ratio of crystallization enthalpy (ΔH_c) with respect to ΔH^0.

Thermogravimetric analysis (TGA) traces were registered on a Q5000 IR thermogravimetric analyzer (TA Instruments-Waters LLC, New Castle, USA) imposing a temperature ramp between 40 and 700 °C at a rate of 10 °C min^{-1} under a constant nitrogen flow of 25 ml min^{-1}. The thermal degradation behavior was quantified on TGA traces by the temperature associated with a weight loss of 2 and 10%, $T_{2wt\%\ loss}$ and $T_{10wt\%\ loss}$, respectively, and the residue value.

2.2.4. Mechanical tests

2.2.4.1. Quasi-static tensile tests. Uniaxial quasi-static tensile tests were performed at room temperature using an Instron® 5966 (Norwood, USA) tensile machine on samples of at least five specimens with cross section of 10.0×4.1 mm^2 and adopting a distance between the grips of 85 mm. Tests were carried out at a crosshead speed of 50 mm·min^{-1}. In accordance to ISO 527 standard, the elastic modulus was measured as a secant value between deformation levels of 0.05% and 0.25%. Uniaxial tensile properties, such as stress at yield (σ_y) and strain at break (ε_b) were also determined.

2.2.4.2. Dynamic mechanical thermal analyses (DMTA). DMTA tests were carried out in tensile mode with a DMA Q800 testing machine (TA Instruments®, New Castle, USA) on rectangular specimens 25 mm long, 8 mm wide and 0.6 mm thick. The samples were analyzed over a temperature range between −50 °C and 180 °C, imposing a heating rate of 3 °C min^{-1} in nitrogen atmosphere and setting frequencies of 1 and 10 Hz. The amplitude of the dynamic deformation of 1 μm was set for each test. The most important viscoelastic functions (E', E'', $tan(\delta)$) were recorded at different temperatures. Using the same apparatus, short term (3600 s) tensile creep tests at 30 °C were also performed at a constant applied stress (σ_0) of 4 MPa. The latter value was at around 10% of the stress at yield of the unfilled PP.

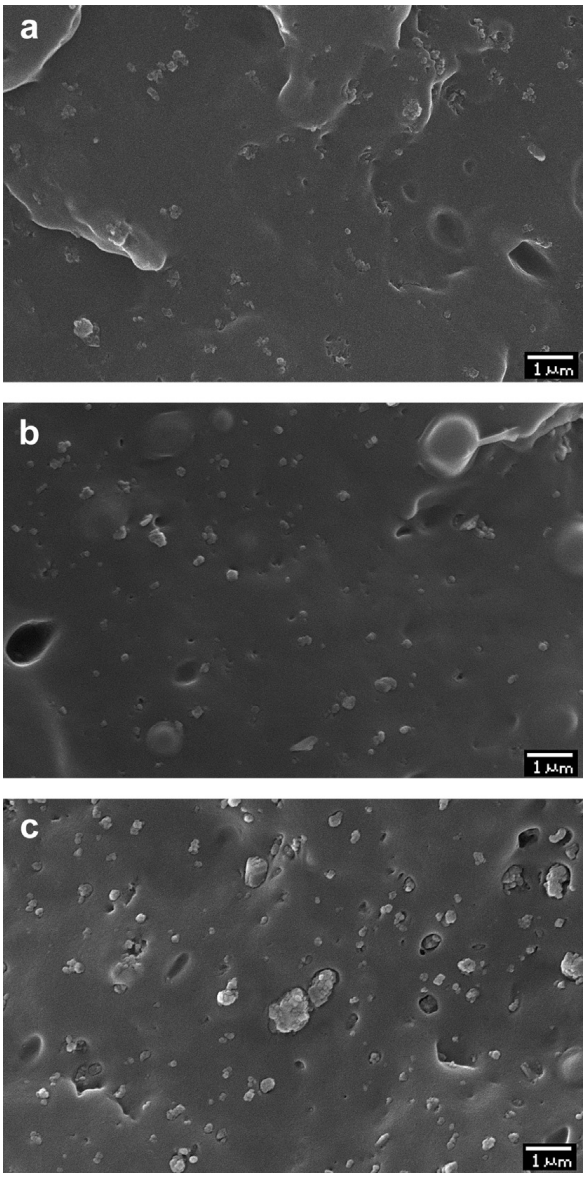

Fig. 1. SEM images of the cryo-fractured surfaces of (a) PP/5BA40, (b) PP/5BA40-OS and (c) PP/10BA40-OS nanocomposites.

2.2.4.3. Elmendorf-type tear tests. Propagation tear tests were performed using an Elmendorf-type tester ED30 (Ceast®, Torino, Italy) on film specimens (thickness of about 0.6 mm) following the standard ISO 6383-2. The tests were carried out on at least five specimens cut from the blow-molded film along the machine and transverse directions, respectively. The propagation tear resistance was measured as the ratio of force (expressed in mN) required to propagate tearing across the specimen with respect to the specimen thickness (expressed in μm). The force reading

was corrected by a multiplication factor of 0.10197 in order to be converted in g μm^{-1}.

3. Results and discussion

3.1. Morphology

SEM pictures taken from the cryo-fractured surface of PP containing the same amount (5 wt%) of BA40 and BA40-OS nanoparticles are given in Fig. 1a–b. BA particles appear quite well dispersed in the PP nanocomposite filled with untreated BA particles, although some agglomerates with average sizes of 300–400 nm are recognizable. The compounding process seems to be effective even in the case of untreated particles, resulting in a good deagglomeration and rather uniform dispersion of the BA nanoparticles. Furthermore, some cavities and humps on a micronscale are observable on the fracture surface, which can be attributed to the rubber (i.e. ethylene-propylene) phase of the PP copolymer (Fig. 1a). On the other hand, the filler dispersion within the polymer matrix is only slightly improved by surface functionalization with silane coupling agent. In fact, the BA nanofiller appears to be organized in smaller and more uniformly distributed BA aggregates in the matrix (Fig. 1b).

BA nanoparticles remain finely dispersed also when added in higher amounts. In fact, Fig. 1c reveals good submicrometer size filler dispersion for the PP containing 10 wt% of BA40-OS nanoparticles. The SEM pictures substantiate that BA nanoparticles can be finely dispersed in PP up to 10 wt%, even when no surface functionalization is applied on the filler or polymeric compatibilizer is added to the matrix.

WAXS patterns of BA nanopowders showed that no crystallinity change occurred due to surface treatment applied (Fig. 2a). Moreover, WAXS performed on PP nanocomposites indicated no significant variation in the crystalline structure of PP due to incorporation of BA with and without surface treatments (Fig. 2b). This is in line with the crystallinity values derived from DSC scans, as will be shown later (cf. Table 1).

3.2. Thermal properties

Since the matrix crystallinity may have an influence on the mechanical properties of nanocomposites, DSC experiments were carried out in order to investigate the crystallization and melting behavior of PP/BA nanocomposites. Incorporation of the filler produces a moderate increase of the crystallization peak temperature for all kinds of BAs, but no particular dependence of the nucleating effect as a function of the BA type was evident (Table 1). Interestingly, the crystallization peak temperature only slightly increases with the addition of BA40-OS2, when compared to composites containing BA40 and BA40-OS. This may be probably due to increased interaction between matrix and BA40-OS2 nanoparticles, which may retard the migration of the PP chains onto the growing crystal nucleus.

The weak nucleation effect of BA is observable more clearly when $T_{c,initial}$ instead of $T_{c,max}$ values are considered. While the data obtained from the first scan might suggest

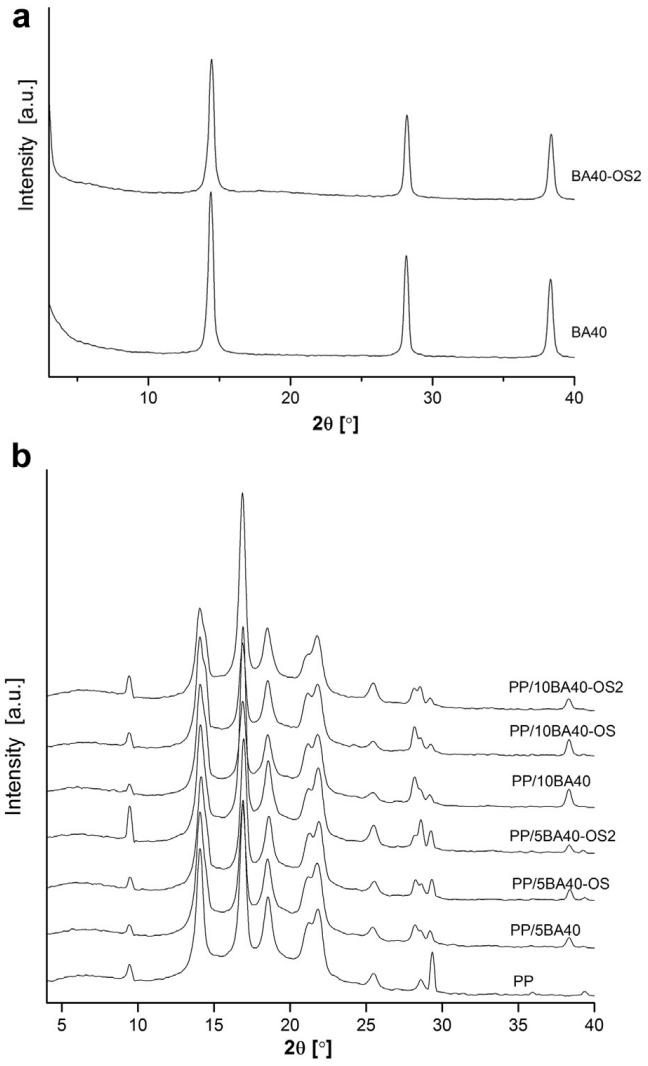

Fig. 2. Wide-angle X-ray diffractograms of (a) BA40 nanopowders and (b) PP nanocomposites filled with 5 and 10 wt% BA versions. The curves were shifted vertically.

that BA increased the crystallinity of PP in the corresponding nanocomposites, the results from the second heating stage do not confirm this effect. Note that the latter data are more relevant as they reflect samples with the same thermal history. The melting behavior was practically not affected by BA incorporation.

The thermal resistance parameters, as detected in TGA measurements, are reported in Table 2. Both $T_{2wt\%\ loss}$ and $T_{10wt\%\ loss}$ noticeably increase with the filler content in all PP/BA40 nanocomposites, showing a slightly higher efficiency in PP/BA40-OS2 samples. This effect could also be linked with the dehydration process of BA nanofiller which delays the polymer degradation. Indeed, TGA analyses conducted on the fillers BA40 and BA40-OS alone show a comparable residue value slightly above 80%, probably indicating the loss of crystal water. On the other hand, the residue value recorded for the filler BA40-OS2 is lower (63.7%), probably due to the loss of part of the organic surface treatment. Representative TGA traces are depicted in Fig. 3 for PP and PP/BA40 nanocomposites. Improved thermal and thermo-oxidative stability due to the addition

Table 1
Melting and crystallization characteristics of PP and relative nanocomposites from DSC measurements.

Sample	First melting			Crystallization			Second melting		
	$T_{m,max}$ [°C]	$T_{m,final}$ [°C]	χ_m [%]	$T_{c,max}$ [°C]	$T_{c,initial}$ [°C]	χ_c [%]	$T_{m,max}$ [°C]	$T_{m,final}$ [°C]	χ_m [%]
PP	166.7	174.6	35.2	122.2	129.8	37.8	167.3	174.8	38.2
PP/2.5BA40	166.6	173.8	37.1	123.0	130.2	38.6	168.3	175.6	38.8
PP/5BA40	166.6	173.9	36.9	124.1	131.0	39.4	166.9	174.4	40.1
PP/10BA40	166.1	173.8	38.3	129.8	135.6	40.6	167.6	174.0	40.3
PP/2.5BA40-OS	166.1	172.7	36.8	123.9	130.0	38.8	167.0	173.6	39.2
PP/5BA40-OS	165.5	173.1	39.5	124.3	130.1	39.2	166.5	173.3	39.4
PP/10BA40-OS	166.9	174.6	40.2	127.5	133.1	39.6	167.9	174.8	39.5
PP/2.5BA40-OS2	167.9	177.2	37.4	122.3	130.1	38.4	168.1	177.3	38.6
PP/5BA40-OS2	167.5	176.1	40.9	122.7	130.2	39.2	167.6	176.4	39.0
PP/10BA40-OS2	167.9	177.8	39.6	123.0	130.5	39.6	168.4	177.8	39.3

of BA has been already reported for PEs [19], PP [35,36] and linear low density polyethylene [37]. It was recently demonstrated on LDPE/BA nanocomposites that the improved resistance of the thermo-oxidative stability due to BA filling is exclusively of physical origin and linked with the barrier effect of the nanoparticles hampering the diffusion of the gaseous degradation products [38].

3.3. Tensile mechanical behavior

The addition of BA40 nanoparticles increases the elastic modulus of the PP matrix, reaching a change of 15% for systems filled with 10 wt% of nanofiller, compared to unfilled PP (Table 3). The stiffening effect induced by nanofiller incorporation is usually attributed to the formation of a rigid interphase between the matrix and the particles. Nevertheless, it has also been recently proposed that nanoparticles aggregation can be another mechanism responsible for stiffness increase in polymer nanocomposites [39,40]. When the properties at yield and at break of the PP/BA40 composites are considered with respect to the unfilled matrix, it can be observed that the yield strength slightly increases, while the elongation at break is also enhanced, reaching a maximum for a filler content of 2.5 wt%. Similar behavior was reported by Khumalo et al. for the tensile yield and elongation at break of HDPE/BA nanocomposites [20]. In particular, the enhanced ductility can be explained by a failure mode in which particle debonding with massive voiding occurs first, followed by void coalescence associated with matrix fibrillation [20].

The addition of BA40-OS nanoparticles results in a remarkable enhancement of the material ductility, producing an increase in strain at break of 163% for the system PP/5BA40-OS, while elastic modulus and yield strength only slightly increase. The increased ductility shown in PP/BA40-OS composite can be mainly attributed to the improved adhesion between PP and BA40–OS which promotes more dissipative failure mode mechanisms.

Nanocomposites with BA40-OS2 show the highest enhancement in yield strength with respect to the other systems. On the other hand, nanofiller addition produces a noticeable decrease in strain at break, probably because of strong interaction between filler and matrix [12]. Although an increase was expected as a result of smaller agglomerations, the opposite happened. It seems that the sulphonic acid surface treatment of BA promotes greater interaction between matrix and particles. As a result, the BA nanoparticles do not participate in massive debonding followed by fibrillation which inhibits the macroscopic elongation of the corresponding nanocomposite [33].

Table 2
TGA parameters on PP and relative nanocomposites.

Sample	$T_{2wt\%\ loss}$[a] [°C]	$T_{10wt\%\ loss}$[b] [°C]	Residue [%]
PP	382.6	430.0	0.3
PP/2.5BA40	383.5	431.7	2.9
PP/5BA40	388.7	437.2	4.4
PP/10BA40	393.4	442.6	9.5
PP/2.5BA40-OS	384.6	432.8	2.7
PP/5BA40-OS	388.5	437.6	4.6
PP/10BA40-OS	395.1	445.7	9.8
PP/2.5BA40-OS2	383.6	431.9	2.8
PP/5BA40-OS2	388.1	438.0	4.3
PP/10BA40-OS2	394.0	443.2	9.9
BA40[c]	/	/	81.3
BA40-OS[c]	/	/	83.5
BA40-OS2[c]	/	/	63.7

[a] Temperature associated with a weight loss of 2%.
[b] Temperature associated with a weight loss of 10%.
[c] Sample in form of nanopowder.

3.4. Viscoelastic behavior

The dynamic-mechanical response of PP is markedly affected by the addition of BA40 nanoparticles. In

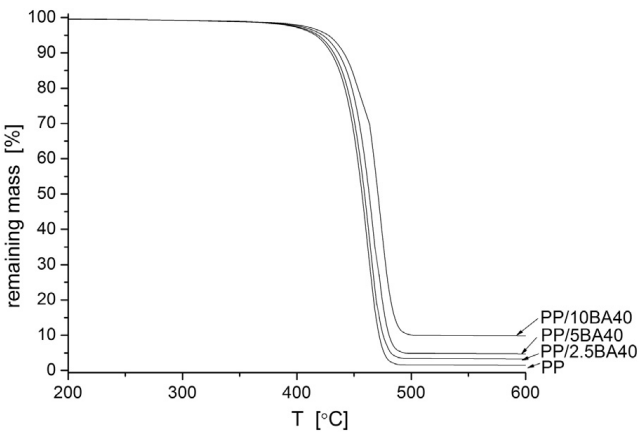

Fig. 3. Remaining mass as a function of temperature during TGA analysis performed on PP and PP/BA40 nanocomposites with different filler contents.

Table 3
Quasi-static tensile mechanical properties and propagation tear resistance of PP nanocomposites.

Sample	Tensile modulus [MPa]	Tensile stress at yield [MPa]	Elongation at break [%]	Tear [g/μm]	
				M.D.[a]	T.D.[b]
PP	901 ± 9	28.5 ± 0.4	127 ± 11	21.5 ± 0.9	24.1 ± 0.8
PP/2.5BA40	987 ± 15	30.2 ± 0.2	168 ± 18	16.5 ± 0.5	27.6 ± 3.5
PP/5BA40	1020 ± 32	30.4 ± 0.5	153 ± 18	15.8 ± 0.7	17.6 ± 0.4
PP/10BA40	1034 ± 25	30.2 ± 0.2	149 ± 28	10.0 ± 1.0	15.2 ± 1.4
PP/2.5BA40-OS	962 ± 34	28.9 ± 0.4	253 ± 103	22.5 ± 1.1	42.9 ± 2.0
PP/5BA40-OS	930 ± 5	29.0 ± 0.2	334 ± 87	14.6 ± 0.8	45.9 ± 6.0
PP/10BA40-OS	[c]	[c]	[c]	14.3 ± 0.9	34.0 ± 10.2
PP/2.5BA40-OS2	920 ± 18	31.4 ± 0.5	136 ± 26	11.0 ± 1.5	12.9 ± 2.0
PP/5BA40-OS2	933 ± 19	30.8 ± 0.6	116 ± 13	/	/
PP/10BA40-OS2	919 ± 3	29.6 ± 0.3	105 ± 41	/	/

[a] Machine direction.
[b] Transverse direction.
[c] No possibility of obtaining specimens for tensile mechanical testing.

particular, the storage modulus (E') increases remarkably as the BA40 content increases, probably due to the restrictions of the molecular chain motion (Table 4). Comparison plots of the storage modulus (E') and loss factor ($tan\delta$) evaluated at 1 Hz are displayed in Fig. 4a and Fig. 4b, respectively, as a function of temperature for unfilled PP and its nanocomposites containing 10 wt% BA. Accordingly, the material's stiffness and load bearing capability increase. The addition of BA40 produces the highest enhancement in E', when compared to the other nanocomposites. Nanofiller incorporation also results in a significant increase of the loss modulus (E''). The glass transition temperature (T_g), evaluated in correspondence of the tan δ peak, was slightly higher for PP/BA40 nanocomposites with respect to unfilled PP, indicating the restriction of the motion of polymer chains induced by the nanofillers incorporation. As expected, DMTA measurements conducted at a frequency of 10 Hz, show higher moduli values but slightly lower T_g and $tan(\delta)$ peak values.

The stiffness of PP/BA40-OS nanocomposites was lower than the reference PP in the whole temperature range studied, in accordance with results of quasi-static tensile tests. Interestingly, incorporation of BA40-OS particles resulted in a slight increase in the T_g, probably indicating effective interfacial interaction between the BA nanoparticles and the PP matrix [9]. Incorporation of PP/BA40-OS2 particles results in a remarkable increase in stiffness at a content of 2.5 wt%, while a progressive decrease occurs at higher filler amounts. These results are in good agreement with the modulus trend observed in quasi-static tensile tests.

In Fig. 5, the isothermal creep compliance of PP and PP/10BA40 nanocomposites, under a constant load of 4 MPa at 30 °C, is reported, while in Table 4 the total creep

Table 4
Creep compliance data and dynamic mechanical properties of PP and relative nanocomposites evaluated at 1 Hz (upper value) and 10 Hz (lower value).

Sample	E′ (−50 °C) [a] [MPa]	E′ (+23 °C) [b] [MPa]	E″ (+23 °C) [c] [MPa]	$T_{\beta_{peak}}$ [d] [°C]	Tan δ [e] ·10^{-2}	$D_{tot,3600s}$ [f] [GPa^{-1}]
PP	5160	2316	151	8.8	6.7	2.04
	5250	2300	147	8.4	7.1	
PP/2.5BA40	5030	1980	122	9.3	6.6	1.79
	5310	2260	124	8.4	6.4	
PP/5BA40	5380	2110	128	10.8	6.8	1.65
	5520	2240	132	8.5	6.5	
PP/10BA40	6830	3020	173	11.9	7.1	1.57
	6930	2870	174	9.3	7.0	
PP/2.5BA40-OS	4110	1990	135	8.4	7.0	1.89
	4500	2110	131	8.2	7.0	
PP/5BA40-OS	3670	1630	122	9.2	8.5	2.14
	3890	1720	124	9.1	8.5	
PP/10BA40-OS	4790	1960	112	9.5	6.4	1.64
	5060	2070	111	9.4	6.3	
PP/2.5BA40-OS2	5510	2210	161	7.4	6.9	2.10
	5720	2440	163	7.9	6.5	
PP/5BA40-OS2	5300	1860	155	9.9	9.6	/[g]
	5530	2000	163	9.6	9.3	
PP/10BA40-OS2	3720	1450	131	10.0	10.8	/[g]
	3910	1560	134	9.7	10.0	

[a] Storage modulus at −50 °C.
[b] Storage modulus at +23 °C.
[c] Loss modulus at +23 °C.
[d] Temperature of β peak recorded in tan δ plots.
[e] Value of loss factor recorded in correspondence of the β peak.
[f] Creep compliance recorded at 3600 s.
[g] No possibility of obtaining specimens for mechanical testing due to problems of bubble formation encountered during the production process.

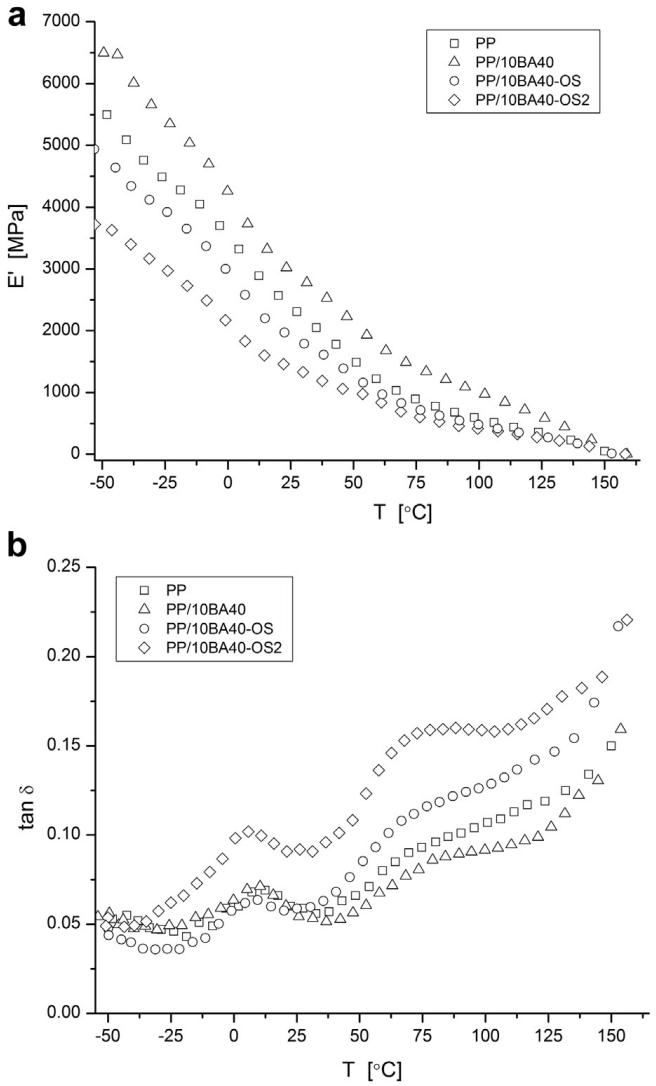

Fig. 4. Dynamic mechanical properties of PP and its nanocomposites (f = 1 Hz): (a) Storage modulus (E') and (b) Loss tangent ($tan(\delta)$) as a function of temperature.

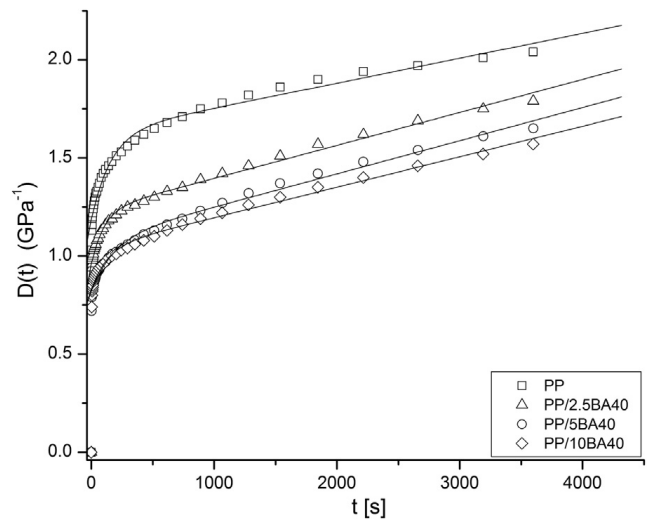

Fig. 5. Creep compliance (D(t)) of PP and PP/BA40 nanocomposites (T = 30 °C, σ_0 = 4 MPa).

compliance after 3600 s ($D_{tot,3600s}$) is given. The introduction of BA nanoparticles results in significant improvement of the creep stability of the material in the case of PP/BA40. It is generally believed that nanoparticles can effectively restrict the motion of polymer chains, influencing the stress transfer at a nanoscale, with positive effects on the creep stability of the material [41]. On the other hand, the addition of BA40-OS nanoparticles leads to lower creep compliance with respect to unfilled PP only at filler contents as high as 10 wt%. Moreover, incorporation of BA40-OS2 filler results in a slightly higher creep compliance when compared to unfilled PP. Since the creep compliance can be factored into the elastic and visco-elastic components, creep results are generally in good agreement with the modulus trend observed in quasi-static tensile tests.

3.5. Propagation tear resistance

Due to orientation during manufacture, plastic films and sheeting frequently show marked anisotropy in their resistance to tearing. This is further complicated by the fact that some films elongate greatly during tearing. The degree of this elongation is dependent on film orientation and the inherent mechanical properties of the polymer [42]. The Elmendorf tearing energy (Fig. 6) of the PP nanocomposites decreased with the BA content for PP/BA40 and PP/BA40-OS2 samples, whereas it was noticeably increased at low BA contents, and gradually decreased for higher filler loadings in PP/BA40-OS composites. Moreover, a marked anisotropy is observable in PP nanocomposites with respect to unfilled PP (Table 3). This effect could occur because of variations in molecular weight distribution due to nanomodification, which produces a change in molecular orientation and, in turn, affects many physical properties included tear strength [43]. However, as already seen in the case of tensile properties, this is not the case. A more probable reason is represented by a higher macro orientation occurring in the nanocomposites during manufacture. Nevertheless, in order to obtain a deeper

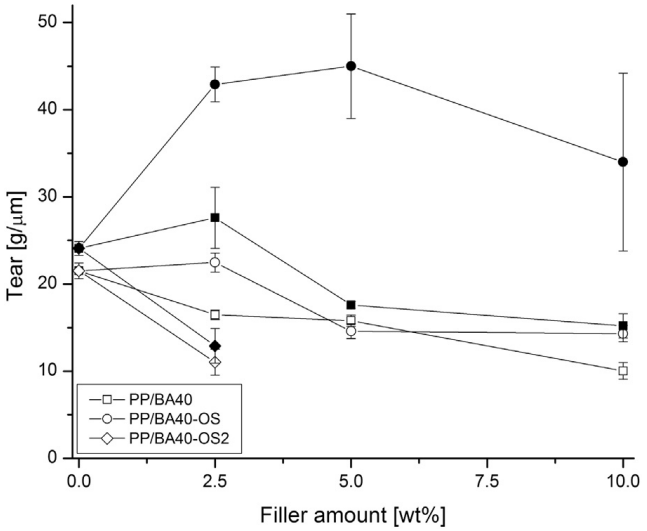

Fig. 6. Propagation tear resistance of PP nanocomposites as a function of the filler content along the machine (open symbol) and transverse (full symbol) direction.

understanding of this phenomenon, further investigations would be required.

It is noteworthy that results of tear resistance are in good agreement with values of strain at break obtained in tensile tests.

The microvoid formation might be responsible for the increment in toughness in PP/BA40-OS samples. As already observed by Soundararajah et al. [44] in the case of poly(-vinyl alcohol) nanomodified with montmorillonite, these microvoids contribute to release the plastic constraint in the matrix, triggering large-scale plastic deformation with consequent tearing of matrix ligaments between microvoids. Moreover, the higher the filler content, the larger the aggregates and agglomerates, resulting in brittle fracture and limiting the microvoid formation. On the other hand, only shear yielding and crazing contribute to energy absorption in neat PP, while in nanocomposites an additional mechanisms is present due to microvoid formation [44].

Interestingly, the incorporation of BA40-OS2 particles results in a prominent decrease in tear resistance, probably due to the greater interaction established between matrix and particles which strongly inhibits the deformation and tearing capabilities of the nanocomposites. Unfortunately, no tear results were available for the PP/5BA40-OS2 and PP/10BA40-OS2 samples, as the formation of a great amount of bubbles during the film processing severely limited the possibility of obtaining wide enough specimens for tear testing.

4. Conclusions

The effects of boehmite nanoparticles (BA) with different surface treatments on the morphology and thermal, viscoelastic and mechanical behavior of a PP copolymer were investigated. PP/BA nanocomposites containing 2.5, 5 and 10 wt % of BA with and without surface treatments were prepared. The BA nanoparticles were treated with octylsilane (OS) and with sulphonic acid compound (OS2). The incorporation of surface treated nanoparticles resulted in slightly better dispersion of the filler within the matrix, as confirmed by SEM observations.

BA acted as a weak nucleation agent in PP matrix, producing slight increases in crystallinity and in the crystallization temperature. By contrast, a substantial enhancement of the degradation properties took place thanks to the nanomodification.

The increased tensile modulus recorded in PP/BA composites was associated with a slight enhancement of the elongation at break. PP/BA-OS systems showed a remarkable increase in ductility with filler introduction, whereas the incorporation of BA-OS2 particles yielded a less ductile material. This was explained by differences in the filler/matrix interactions governing the failure sequence and mode. The observations regarding tensile tests were in line with the changes observed for the storage and loss modulus in DMTA tests and creep resistance. The propagation tear resistance increased at low filler contents in the case PP/BA-OS composites. In this case, the nucleation of microvoids had a positive effect in the enhancement of tearing energy while the agglomeration of BA particles had a negative effect.

Acknowledgement

This work was performed in the framework of a bilateral cooperation agreement between Italy (HU11MO8) and Hungary (TÉT_10-1-2011-0218).

References

[1] F. Tuba, V.M. Khumalo, J. Karger-Kocsis, Essential work of fracture of poly(epsilon-caprolactone)/boehmite alumina nanocomposites: effect of surface coating, J. Appl. Polym. Sci. 129 (5) (2013) 2950.
[2] W. Brostow, T. Datashvili, B. Huang, J. Too, Tensile properties of LDPE + boehmite composites, Polym. Compos. 30 (6) (2009) 760.
[3] K.-S. Lee, Y.-W. Chang, Thermal, mechanical, and rheological properties of poly(e-caprolactone)/halloysite nanotube nanocomposites, J. Appl. Polym. Sci. 1 (2012).
[4] A. Durmus, A. Kasgöz, C. Macosko, Mechanical properties of linear low-density polyethylene (LLDPE)/clay nanocomposites: estimation of aspect ratio and interfacial strength by composite models, J. Macromol. Sci. B 47 (3) (2008) 608.
[5] A. Durmus, A. Kasgöz, C.W. Macosko, Linear low density polyethylene (LLDPE)/clay nanocomposites. Part I: structural characterization and quantifying clay dispersion by melt rheology, Polymer 48 (15) (2007) 4492.
[6] S. Hotta, D.R. Paul, Nanocomposites formed from linear low density polyethylene and organoclays, Polymer 45 (22) (2004) 7639.
[7] A. Dorigato, A. Pegoretti, A. Frache, Thermal stability of high density polyethylene–fumed silica nanocomposites, J. Therm. Anal. Calorim 109 (2) (2012) 863.
[8] P. Kiliaris, C.D. Papaspyrides, Polymer/layered silicate (clay) nanocomposites: an overview of flame retardancy, Prog. Polym. Sci. 35 (7) (2010) 902.
[9] M.Z. Rong, M.Q. Zhang, S.L. Pan, B. Lehmann, K. Friedrich, Analysis of the interfacial interactions in polypropylene/silica nanocomposites, Polym. Int. 53 (2) (2004) 176.
[10] R.-J. Zhou, T. Burkhart, Polypropylene/SiO_2 nanocomposites filled with different nanosilicas: thermal and mechanical properties, morphology and interphase characterization, J. Mater. Sci. 46 (5) (2010) 1228.
[11] H. Zou, S. Wu, J. Shen, Polymer/Silica nanocomposites: preparation, characterization, properties, and applications, Chem. Rev. 108 (2008) 3893.
[12] D.N. Bikiaris, A. Vassiliou, E. Pavlidou, G.P. Karayannidis, Compatibilisation effect of PP-g-MA copolymer on iPP/SiO_2 nanocomposites prepared by melt mixing, Eur. Polym. J. 41 (9) (2005) 1965.
[13] S.-P. Liu, J.-R. Ying, X.-P. Zhou, X.-L. Xie, Y.-W. Mai, Dispersion, thermal and mechanical properties of polypropylene/magnesium hydroxide nanocomposites compatibilized by SEBS-g-MA, Compos. Sci. Technol. 69 (11–12) (2009) 1873.
[14] H. Mirzazadeh, A.A. Katbab, A.N. Hrymak, The role of interfacial compatibilization upon the microstructure and electrical conductivity threshold in polypropylene/expanded graphite nanocomposites, Polym. Adv. Technol. 22 (6) (2011) 863.
[15] B. Mohebby, P. Fallah-Moghadam, A.R. Ghotbifar, S. Kazemi-Najafi, Influence of maleic-anhydride-polypropylene (mapp) on wettability of polypropylene/wood flour/glass fiber hybrid composites, J. Agriculture Sci. Technol. 13 (6) (2011) 877.
[16] O. Lin, Z. Mohd Ishak, H. Akil, Preparation and properties of nanosilica-filled polypropylene composites with PP-methyl POSS as compatibiliser, Mater. Des. 30 (3) (2009) 748.
[17] P. Blaszczak, W. Brostow, T. Datashvili, H.E.H. Lobland, Rheology of low-density polyethylene + boehmite composites, Polym. Compos. 31 (11) (2010) 1909.
[18] C. Özdilek, K. Kazimierczak, S.J. Picken, Preparation and characterization of titanate-modified boehmite–polyamide-6 nanocomposites, Polymer 46 (16) (2005) 6025.
[19] V.M. Khumalo, J. Karger-Kocsis, R. Thomann, Polyethylene/synthetic boehmite alumina nanocomposites: structure, thermal and rheological properties, Expr. Polym. Lett. 4 (5) (2010) 264.
[20] V.M. Khumalo, J. Karger-Kocsis, R. Thomann, Polyethylene/synthetic boehmite alumina nanocomposites: structure, mechanical, and perforation impact properties, J. Mater. Sci. 46 (2) (2010) 422.
[21] C.Y. Chee, N.L. Song, L.C. Abdullah, T.S.Y. Choong, A. Ibrahim, T.R. Chantara, Characterization of mechanical properties: low-density polyethylene nanocomposite using nanoalumina particle as filler, J. Nanomat. 2012 (1) (2012) 1.

[22] E.S. Ogunniran, R. Sadiku, S. Sinha Ray, N. Luruli, Effect of boehmite alumina nanofiller incorporation on the morphology and thermal properties of functionalized poly(propylene)/polyamide 12 blends, Macromol. Mater. Eng. 297 (3) (2012) 237.
[23] C. Özdilek, B. Norder, S.J. Picken, A study of the thermo-mechanical behavior of boehmite-polyamide-6 nanocomposites, Thermoch. Acta 472 (1–2) (2008) 31.
[24] J. Zhang, Q. Ji, P. Zhang, Y. Xia, Q. Kong, Thermal stability and flame-retardancy mechanism of poly(ethylene terephthalate)/boehmite nanocomposites, Polym. Degrad. Stab. 95 (7) (2010) 1211.
[25] K. Das, S. Sinha Ray, S. Chapple, J. Wesley-Smith, Mechanical, thermal, and fire properties of biodegradable polylactide/boehmite alumina composites, Ind. Eng. Chem. Res. 52 (18) (2013) 6083.
[26] X. Liu, Q. Wu, PP/clay nanocomposites prepared by grafting-melt intercalation, Polymer 42 (2001) 10013.
[27] K. Prashantha, Processing and characterization of halloysite nanotubes filled polypropylene nanocomposites based on a masterbatch route: effect of halloysites treatment on structural and mechanical properties, Express Polym. Lett. 5 (4) (2011) 295.
[28] A. Askeland, Hiroyuki Fukushima, Inhwan Do, K. Kalaitzidou, L.T. Drzal, Exfoliated graphite nanoplatelets [2] surface treatment, in: NSTI-Nanotech, 1, 2006, p. 76.
[29] A. Fina, H.C.L. Abbenhuis, D. Tabuani, A. Frache, G. Camino, Polypropylene metal functionalised POSS nanocomposites: a study by thermogravimetric analysis, Polym. Degrad. Stab. 91 (5) (2006) 1064.
[30] T. Kuila, S. Bose, A.K. Mishra, P. Khanra, N.H. Kim, J.H. Lee, Chemical functionalization of graphene and its applications, Prog. Mater. Sci. 57 (7) (2012) 1061.
[31] P. Steurer, R. Wissert, R. Thomann, R. Mulhaupt, Functionalized graphenes and thermoplastic nanocomposites based upon expanded graphite oxide, Macromol. Rapid Commun. 30 (4–5) (2009) 316.
[32] E.S. Ogunniran, R. Sadiku, S. Sinha Ray, N. Luruli, Morphology and thermal properties of compatibilized PA12/PP blends with boehmite alumina nanofiller inclusions, Macromol. Mater. Eng. 297 (7) (2012) 627.
[33] D. Pedrazzoli, F. Tuba, V. Khumalo, J. Karger-Kocsis, A. Pegoretti, Mechanical and rheological response of polypropylene/boehmite nanocomposites, J. Reinf. Plast. Compos 33 (3) (2014) 268.
[34] E. James, Polymer Data Handbook, Oxford University Press, 1999.
[35] R.C. Streller, R. Thomann, O. Torno, R. Mülhaupt, Isotactic poly(-propylene) nanocomposites based upon boehmite nanofillers, Macromol. Mater. Eng. 293 (3) (2008) 218.
[36] S. Bocchini, S. Morlat-Thérias, J.-L. Gardette, G. Camino, Influence of nanodispersed boehmite on polypropylene photooxidation, Polym. Degrad. Stab 92 (10) (2007) 1847.
[37] D. Pedrazzoli, R. Ceccato, J. Karger-Kocsis, A. Pegoretti, Viscoelastic behaviour and fracture toughness of linear-low-density polyethylene reinforced with synthetic boehmite alumina nanoparticles, Express Polym. Lett. 7 (8) (2013) 652.
[38] E. Vuorinen, N. Nhlapo, T. Mafa, J. Karger-Kocsis, Thermooxidative degradation of LDPE nanocomposites: effect of surface treatments of fumed silica and boehmite alumina, Polym. Degrad. Stab. 98 (11) (2013) 2297.
[39] A. Dorigato, Y. Dzenis, A. Pegoretti, Nanofiller aggregation as reinforcing mechanism in nanocomposites, Procedia Eng. 10 (2011) 894.
[40] A. Dorigato, A. Pegoretti, Y. Dzenis, Filler aggregation as a reinforcement mechanism in polymer nanocomposites, Mechanics Mater. 61 (2013) 79.
[41] F. Bondioli, A. Dorigato, P. Fabbri, M. Messori, A. Pegoretti, Improving the creep stability of high density polyethylene by acicular titania nanoparticles, J. Appl. Polym. Sci. 112 (2) (2009) 1045.
[42] A. D1922-09, Standard Test Method for Propagation Tear Resistance of Plastic Film and Thin Sheeting by Pendulum Method, 2009.
[43] A.J. Peacock, A. Calhoun, Polymer Chemistry: Properties and Applications, 2006.
[44] Q.Y. Soundararajah, B.S.B. Karunaratne, R.M.G. Rajapakse, Mechanical properties of poly(vinyl alcohol) montmorillonite nanocomposites, J. Compos. Mater. 44 (3) (2009) 303.